Ultrasonics 49 (2009) 112–119

Contents lists available at ScienceDirect

Ultrasonics

journal homepage: www.elsevier.com/locate/ultras

Spatial confinement of ultrasonic force fields in microfluidic channels

Otto Manneberg [a], S. Melker Hagsäter [b], Jessica Svennebring [a], Hans M. Hertz [a], Jörg P. Kutter [b], Henrik Bruus [b], Martin Wiklund [a,*]

[a] Biomedical and X-ray Physics, Royal Institute of Technology, KTH-AlbaNova, SE-106 91 Stockholm, Sweden
[b] Department of Micro- and Nanotechnology, Technical University of Denmark, DTU Nanotech, Building 345 East, DK-2800 Kongens Lyngby, Denmark

ARTICLE INFO

Article history:
Received 21 January 2008
Received in revised form 9 June 2008
Accepted 19 June 2008
Available online 8 July 2008

PACS:
43.25.Gf

Keywords:
Ultrasonic manipulation
Acoustic radiation force
Microfluidic chip
Particle image velocimetry
Spatial confinement
Cell handling

ABSTRACT

We demonstrate and investigate multiple localized ultrasonic manipulation functions in series in microfluidic chips. The manipulation functions are based on spatially separated and confined ultrasonic primary radiation force fields, obtained by local matching of the resonance condition of the microfluidic channel. The channel segments are remotely actuated by the use of frequency-specific external transducers with refracting wedges placed on top of the chips. The force field in each channel segment is characterized by the use of micrometer-resolution particle image velocimetry (micro-PIV). The confinement of the ultrasonic fields during single- or dual-segment actuation, as well as the cross-talk between two adjacent fields, is characterized and quantified. Our results show that the field confinement typically scales with the acoustic wavelength, and that the cross-talk is insignificant between adjacent fields. The goal is to define design strategies for implementing several spatially separated ultrasonic manipulation functions in series for use in advanced particle or cell handling and processing applications. One such proof-of-concept application is demonstrated, where flow-through-mode operation of a chip with flow splitting elements is used for two-dimensional pre-alignment and addressable merging of particle tracks.

1. Introduction

Ultrasonic standing wave (USW) manipulation technology in microfluidic chips has recently emerged as a powerful tool for, e.g., continuous alignment, separation, trapping and aggregation of micrometer-sized particles or cells [1,2]. We have previously shown that it is possible to generate independent standing wave fields in different directions inside a microfluidic channel, where each field is addressed by a specific external transducer [3]. However, a remaining problem is that USW manipulation technology has poor spatial localization in comparison to alternative contactless manipulation methods such as dielectrophoresis [4] and optical tweezers [5]. In the present paper, we demonstrate for the first time multiple spatially separated and confined ultrasonic force fields by microchannel design, with the aim of developing more advanced and complex lab-on-a-chip systems based on USW technology.

One characteristic of the present USW manipulation technology (that differs from the characteristics of dielectrophoresis and optical tweezers), is the possibility to generate a uniform force field in the entire fluid channel in a chip. For example, with USW technology it is possible to guide a particle or a cell through a microfluidic chip at constant velocity and without any contact with the channel walls [3], or to separate particles from a suspension at high flow rates [2]. On the other hand, dielectrophoresis has been used in more complex particle or cell processing systems where several manipulation functions are located at different sites along the fluid channel [4]. Here, different micro-electrode geometries define different addressable manipulation functions, each with high spatial accuracy in terms of both localization and confinement of the corresponding dielectrophoretic force field. Thus, advanced single-particle handling and processing systems are realized by combining several consecutive manipulation functions (such as alignment, parking, sorting, separation, etc.) and a continuous driving fluid flow. In comparison to dielectrophoresis, USW technology has a much lower degree of instrumentation complexity [6], and also better prospects for gentle and long-term handling of sensitive cells [7,8]. Therefore, it is of interest to investigate if USW technology can be used in advanced particle processing systems based on combinations of several spatially separated and localized manipulation functions.

To date, several different methods have been suggested for coupling of ultrasound from a transducer into a well-defined standing wave in a microfluidic chip. The standard approach is based on the one-dimensional resonator that consists of a stack of plane-parallel layers: a PZT layer, a coupling layer, a fluid layer and a reflecting layer [7,9,10], or with the reflecting layer exchanged for another

* Corresponding author. Tel.: +46 8 5537 8134; fax: + 46 8 5537 8466.
E-mail address: martin@biox.kth.se (M. Wiklund).

0041-624X/$ - see front matter © 2008 Elsevier B.V. All rights reserved.
doi:10.1016/j.ultras.2008.06.012

coupling layer and PZT layer [11,12]. However, it has been shown that in silicon/glass-based microfluidic chips, it is not of critical importance how the system is excited. For example, one reported method is based on exciting the channel perpendicularly to the outgoing wave from an external transducer [2]. An alternative approach, developed in our lab, is based on oblique coupling via a refracting wedge on an external transducer for controlled directing of the incident wave into the fluid channel [6]. Another reported method is based on bending vibrations of a glass plate in contact with the fluid channel [13]. However, all these methods typically result in a standing wave field that extends along the whole fluid channel. Thus, it is difficult to confine an ultrasonic field in a chip by wave propagation from an external transducer only.

We note that by integrating the PZT elements in the fluid channel, localization and confinement of an ultrasonic standing wave field can be obtained [14–16]. In such devices, the extent of the ultrasonic field is similar to the size of the PZT element (typically, 0.5–0.8 mm wide square elements designed for operation around 10 MHz). However, the generated standing wave field has a complicated lateral distribution due to strong near-field effects. Furthermore, the experimental arrangement is more complicated and less flexible than in similar devices using external transducers (e.g., in Refs. 2,6). Another restriction with channel-integrated PZT elements is the limited optical access, which excludes trans-illumination microscopy techniques. Finally, since the PZT element is in direct contact with the fluid inside the microchannel, the biocompatibility may be reduced due to, e.g., heating (cf. Ref. 8).

In the present paper, we demonstrate for the first time spatial localization, separation and confinement of multiple ultrasonic standing wave fields in optically transparent microfluidic chips utilizing remote actuation from external transducers. The method is based on local matching of the channel width to the transducer frequency in chips with non-uniform channel cross-sections. We present results from two different chip designs; one for investigating the dependence of the confinement on small differences in channel width, and one with flow splitting elements designed for two-dimensional alignment and addressable merging of particle tracks. The ultrasonic fields are quantified by the use of micrometer-resolution particle image velocimetry (micro-PIV) [17] during actuation of a single channel segment, or of two adjacent channel segments simultaneously. The results are important for the understanding of how ultrasonic resonances are formed in microfluidic chips, as well as for developing future particle handling systems with tailor-made, localized and confined ultrasonic resonances by microchannel design.

2. Theoretical background

As a basic condition for the design process, we assume that an ultrasonic resonance can be localized and confined through proper matching of the width and height (relative to the acoustic wavelength) of a particular channel segment. Furthermore, we assume that the total three-dimensional resonant field in a chip is a superposition of one-dimensional and spatially harmonic resonances in orthogonal directions, and that each such one-dimensional resonance can be remotely excited by an external frequency-specific transducer. These conditions are the starting point for the theoretical background presented below. However, we are aware that the conditions are simplifications. In reality, the resonances in a microfluidic chip should be regarded as full three-dimensional fields that extend not only in the fluid channel but rather in the whole chip structure. Therefore, the degree of localization and confinement of the field into a particular part of the fluid channel is a function of not only the channel geometry, but also the acoustic impedances and geometries of all supporting layers to the channel structure, including the whole fluid channel itself [18]. The validity of our simplified conditions below is further discussed in Section 5.

2.1. Ultrasonic standing wave manipulation

It has long been known that particles in an ultrasonic standing wave will be subjected to a primary radiation force F_{PR}, which attracts suspended particles to the nodes or antinodes of the standing wave depending on the acoustic properties of the particles relative to the surrounding medium [19]. Gor'kov has shown that the force on a particle of volume V in an arbitrary acoustic field is given by [20]

$$F_{PR} = -V\nabla\left(f_1\frac{\langle p^2\rangle}{2\rho c} - \frac{3}{2}\rho f_2\frac{\langle v^2\rangle}{2}\right) \tag{1}$$

where the brackets denote time-averaging and ρ and c are the density and speed of sound in the medium. f_1 and f_2 are contrast factors which depend on the speed of sound and the density of the medium and particle according to

$$f_1 = 1 - \frac{\rho c^2}{\rho_p c_p^2} \quad \text{and} \quad f_2 = 2\frac{\left(\rho_p - \rho\right)}{2\rho_p + \rho} \tag{2}$$

where the index p indicates "particle". In the simple case of a one-dimensional spatially sinusoidal standing wave in the x direction, Eq. (1) reduces to [20]

$$F_{PR}(x) = \frac{V p_0^2 k}{4\rho c^2}\left(f_1 + \frac{3}{2}f_2\right)\sin(2kx) \tag{3}$$

where k is the wavenumber, defined as $k = 2\pi/\lambda$ where λ is the acoustic wavelength. As mentioned above, a microchip containing a microchannel is a complex resonator. However, to a first approximation, the forces in such a channel can be obtained by simple superposition of plane-parallel resonators in perpendicular directions, each with a force field given by Eq. (3) [21]. This approximation (i.e., assuming no coupling between the orthogonal fields) is sufficiently accurate if the superposed fields do not operate at frequencies that are multiples of each other [22].

2.2. Force field quantification by micro-PIV

In the present work, the primary radiation force field F_{PR} is quantified in two dimensions (x and z, cf. Fig. 1) using the micro-PIV technique, in which the motion of tracer particles in the form of velocity vector fields is acquired from consecutive image frames [17]. F_{PR} is proportional to the bead velocity given that no other forces or flows are present, and that the time after activating a transducer is well above the time constant τ_p for reaching force equilibrium between F_{PR} and the viscous Stokes drag. The time constant τ_p is given by [23]

$$\tau_p = 2\rho_p r_p^2/9\eta \tag{4}$$

where r_p is the radius of the particle and η is the viscosity of the liquid medium. When representing the relative force fields with velocity fields, possible sources of error are, e.g., acoustic streaming [24] and sedimentation by gravity. Acoustic streaming will, through viscous drag, influence the particles with a force proportional to the particle radius r. As F_{PR} is proportional to r^3, the streaming will typically dominate when the particles are small ($r \sim 0.5$ μm) whereas F_{PR} will typically dominate when the particles are larger ($r \sim 5$ μm), as in our experiments. The time constant τ_{sed} for sedimentation a (vertical) distance h in a fluid channel is given by

$$\tau_{sed} = \frac{h}{v_{sed}} = \frac{9\eta h}{2(\rho_p - \rho)r_p^2 g} \tag{5}$$

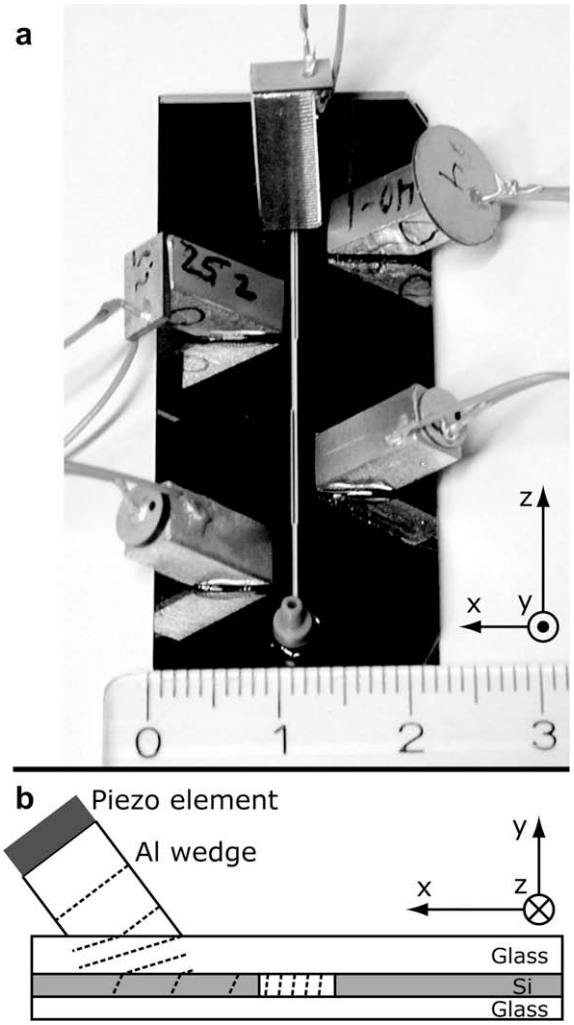

Fig. 1. Photograph (a) and schematic (not to scale) of cross-section (b) of the "Split Chip" with mounted transducers. The ruler scale is in millimeter. In (b), the dashed lines represent wavefronts incident at an angle typical for manipulation in the *x* direction.

where v_{sed} is the sedimentation speed and g is the acceleration of gravity. A typical value of τ_{sed} in our microchannels is 1 minute (for 5-μm-diam. polyamide beads in water, and choosing h as half the channel height), and is therefore of little importance.

2.3. Combined ultrasonic standing wave manipulation and flow

At the employed flow level (~0.1 μL/s) in our flow-through experiments (cf. Section 4.2), the flow is laminar in the whole channel structure (e.g., the Reynolds number is ~1). This means that once the force from the ultrasonic field has positioned a particle in a streamline, it will stay in that streamline until subjected to an external force. In our experiments, we distinguish between a streamline (path of a fluid element) and a particle track (path of a suspended particle).

3. Experimental arrangement

In our experiments, we used two different chip designs (described in detail in the next paragraph). Fig. 1a is a photograph of one of the chips used with mounted transducers and Fig. 1b illustrates the principles of the oblique coupling method (described in Refs. [3,6]). Both chips are fabricated from 51.4 × 22 mm^2 glass-silicon-glass stacks with the microchannel plasma etched into the silicon layer (GeSim, Germany). The bottom glass plate of both chips is 200 μm thick, i.e., close to standard microscope coverslip thickness. This allows investigation of the channel using any kind of high-resolution optical microscopy, including both trans- and epi-illumination techniques. The transducers were fabricated by gluing planar PZT elements (Pz26, Ferroperm, Denmark) to aluminum wedges (cf. Fig. 1a) with a cross-section of 5 × 5 mm^2, and driven at peak-to-peak voltages up to 13 V by separate function generators operating at different frequencies within the range 1.5–7 MHz. The aluminum wedges were attached to the chip (cf. Fig. 1a) using a quick-drying and water-soluble adhesive gel (Tensive, Parker Laboratories, USA).

The channel designs in the two investigated chips are schematically illustrated in Fig. 2. In both designs, the channel height is 110 μm and the widths are specifically designed to spatially confine resonances to a certain part of the channel by matching of width and frequency as to fulfill the simplified resonance condition

$$L = \frac{m}{2}\cdot\lambda = \frac{m}{2}\cdot\frac{c}{f} \tag{6}$$

where L is the channel width in the relevant direction, m is a positive integer, λ is the acoustic wavelength in the fluid, c is the speed of sound in the fluid and f is the acoustic frequency. The first chip (the "Step Chip", cf. Fig. 2a) has a straight channel with three 15-mm long sections of different width (643 μm, 600 μm and 500 μm). This chip is designed to utilize the fields from four different transducers, three of which act to focus particles in the x direction in each of the segments and one to levitate them in the y direction against the force of gravity. The second chip (the "Split Chip") has a more complex channel structure including two flow splitting elements, as illustrated in Fig. 2b. This chip is designed to use the fields from five different transducers operating at different frequencies to excite resonances in different parts of the chip, as indicated in Fig. 2b. Four of these can perform focusing of the particles in the x direction, and one is used to levitate the beads in the y direction. Thus, the operator can choose between merging particle tracks 1 + 2, tracks 2 + 3 or all tracks (cf. Fig. 2b). This principle

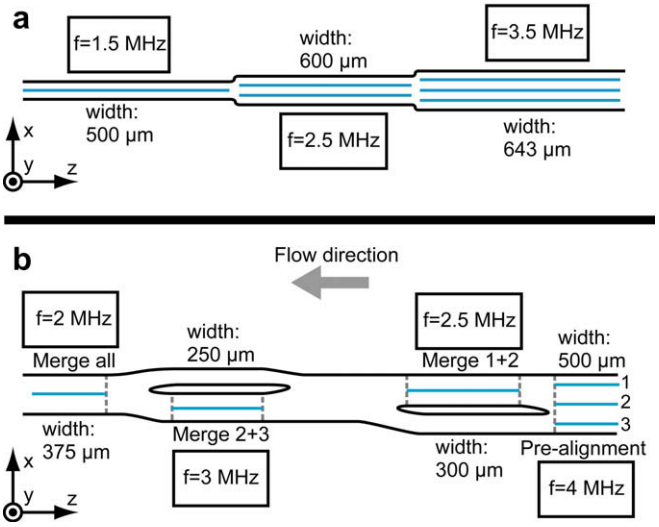

Fig. 2. Schematics (not to scale) top-view of the two employed chips; the "Step Chip" (a) and the "Split Chip" (b). The horizontal lines in the channels indicate the pressure node pattern, i.e., the lines to which particles are focused. The thin dashed lines in (b) mark the boundaries of the spatially confined resonances in each channel segment. The levitator transducers operating at 7.1 MHz is not shown, but is placed to the far right in experiments.

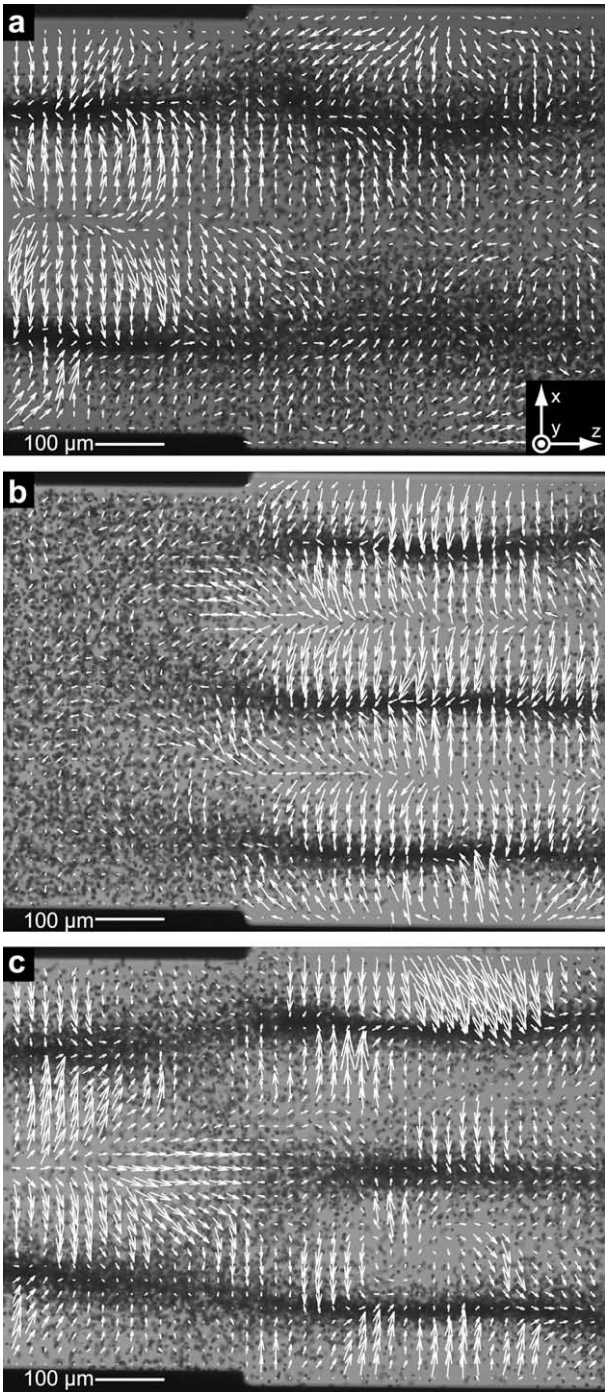

Fig. 3. Characterization of the primary radiation force field F_{PR} in the "Step Chip" (cf. Fig. 2a), measured by micrometer-resolution particle image velocimetry (micro-PIV). Actuation at 2.62 MHz of the left channel segment (a), at 3.51 MHz of the right channel segment (b), and at 2.62 and 3.51 MHz of both channel segments simultaneously (c). White arrows indicate the relative sizes and directions of the forces immediately after actuation is initialized. Dark regions indicate the bead pattern after ~10 s of actuation. The length of the coordinate arrows in (a) corresponds to a velocity of 10 µm/s.

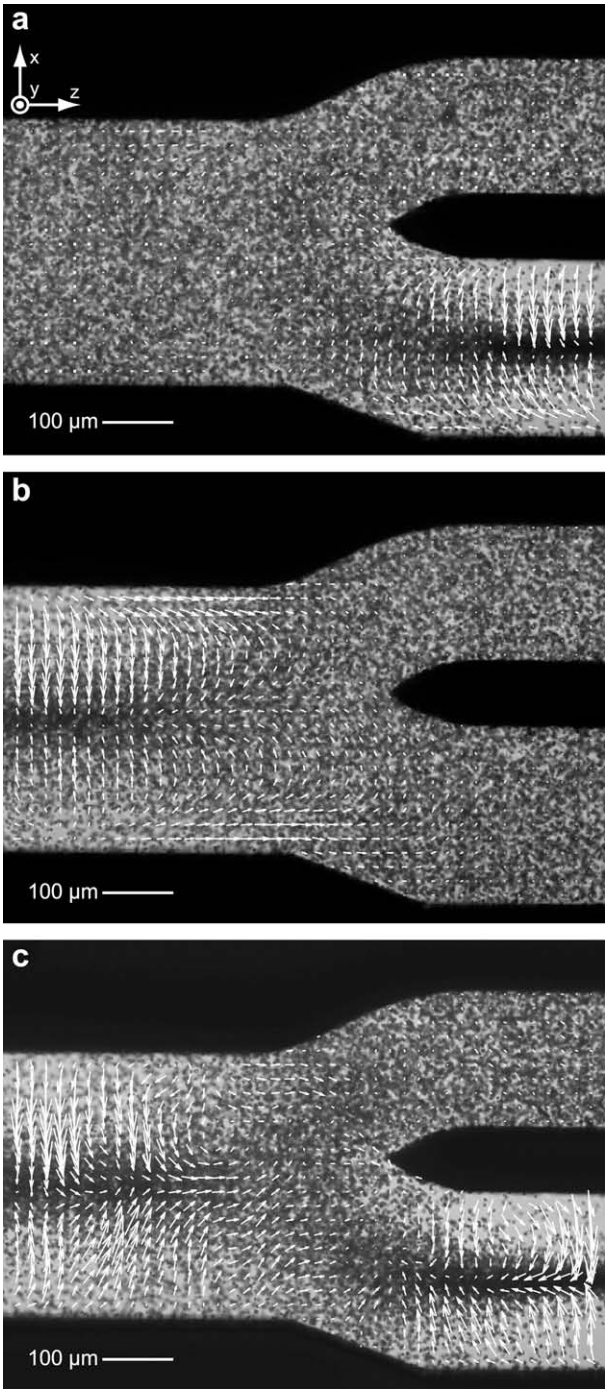

Fig. 4. Characterization of the primary radiation force field F_{PR} in the "Split Chip" (cf. Fig. 2b), measured by micrometer-resolution particle image velocimetry (micro-PIV). Actuation at 2.94 MHz of the lower right channel segment (a), at 2.10 MHz of the left channel segment (b), and at 2.94 and 2.10 MHz of both channel segments simultaneously (c). White arrows indicate the relative sizes and directions of the forces immediately after actuation is initialized. Dark regions indicate the bead pattern after ~10 s of actuation. The length of the coordinate arrows in (a) corresponds to a velocity of 10 µm/s.

could easily be expanded, and more in- or outlets added, to accommodate to the needs of a specific application (cf. Section 5).

Each resonance frequency was identified by tuning the applied transducer frequency in small steps around the expected frequency (according to Eq. 6) and observing the particle manipulation response in the corresponding channel segment. The operating frequency was then manually selected via the optimal ability to position particles quickly and uniformly into the nodes. Micro-PIV measurements were performed at all sites where the channels change width. To investigate the degree of spatial confinement, measurements were made with operation of either of the two or both transducers corresponding to actuation of the channel segments on each sides of the change in channel width (cf. Section

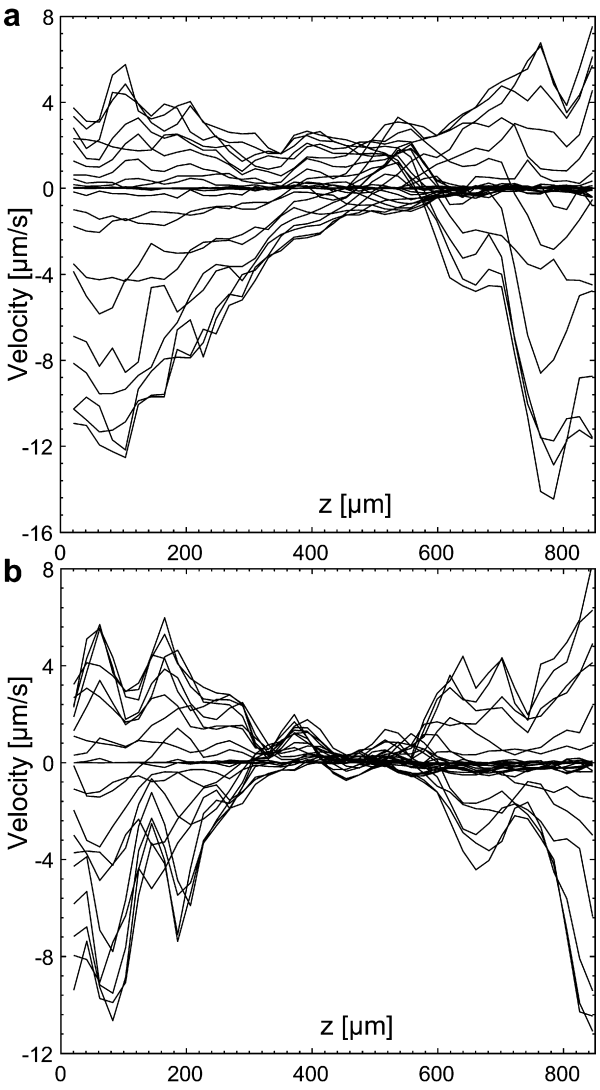

Fig. 5. Quantification of the field confinement and cross-talk in the "Split Chip" (cf. Fig. 4). The diagrams present the *x* components (cf. coordinate system in Fig. 4) of the velocity vectors along 31 *z*-axes equally spaced in the *x* direction. (a) Shows the *x* component of the sum of the velocity fields acquired when actuating the two channel segments separately (cf. Fig. 4a and b). (b) Shows the *x* component of the velocity field acquired when actuating both channel segments simultaneously (cf. Fig. 4c).

4). We also demonstrate flow-through-mode operation with the Split Chip operated with up to four independent transducers simultaneously.

Two different kinds of particles were employed in the experiments;10.4 µm green-fluorescent polystyrene beads (Bangs Labs, USA) for the flow-through experiments and 5 µm polyamide beads (Danish Phantom Design, Denmark) for the micro-PIV investigations. The beads were chosen for their resemblance to cells in both volume and acoustic properties. The beads were diluted in phosphate-buffered saline (PBS), pH 7.4, with 0.05% Tween-20 and introduced into the system by use of a syringe pump and Teflon (FEP) tubing.

In the flow-through-mode experiments (cf. Fig. 6), imaging was performed using an inverted microscope (AxioVert 135 M, Zeiss, Germany) with a 2.5 × /0.075 NA objective and a CCD camera (AxioCam HSc, Zeiss, Germany). In order to visualize both the beads and the microchannel, epi-flourescence and low-level trans-illumination were used simultaneously. For the micro-PIV measurements performed without flow (cf. Figs. 3 and 4), image frames

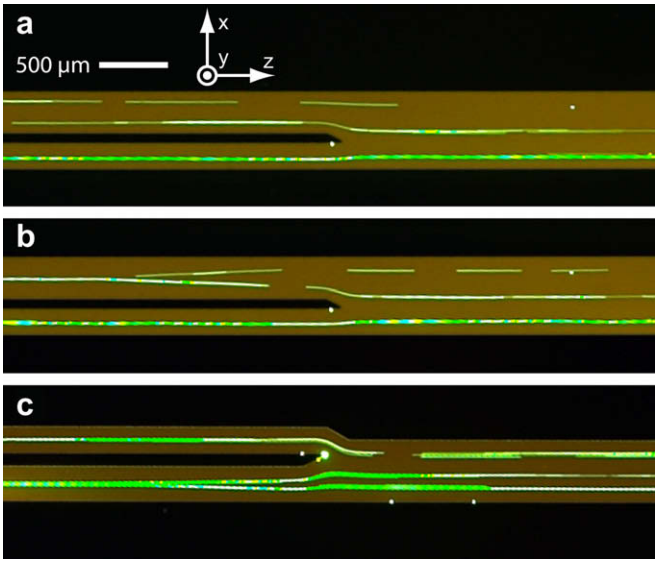

Fig. 6. Demonstration of addressable merging of particle tracks in the "Split Chip". Panels (a) and (b) show the particle tracks without and with actuation of the upper left channel segment, respectively. Panel (c) shows merging of the two lower particle tracks by actuation of the lower left channel segment. The chip site in (a) and (b) is located at the 2.5-MHz transducer, and the chip site in (c) is located at the 3.0-MHz transducer (cf. Fig. 2b).

were recorded in pairs with a CCD camera (HiSense MkII, Dantec Dynamics, Denmark) mounted on an inverted microscope (AxioVert 100, Zeiss, Germany) with a 10 × /0.25 NA objective. The sample was illuminated in back-lit mode by a light emitting diode (K2, Lumileds, USA) [25]. The velocity vector fields were generated using essentially the same protocol as described by Hagsäter et al. [18]. Before each new micro-PIV measurement, the channel was flushed and re-seeded to give a homogenous starting distribution of beads.

4. Results

In this section, we report on micro-PIV results when the two chips (the "Step Chip" and the "Split Chip") are operated without flow during ultrasonic actuation of one or several channel segments. The micro-PIV results are analyzed in order to quantify the spatial separation and confinement of the force fields, and possible cross-talk between two adjacent channel segments. Furthermore, we demonstrate flow-through operation of the Split Chip, which is designed for two-dimensional alignment and addressable merging of particle tracks.

4.1. Micro-PIV measurements

Micro-PIV measurements were made at all sites where the channels change width, both in the Step Chip and in the Split Chip (cf. Fig. 2). However, in order to minimize the number of figures we have chosen to present results from one representative site in each chip, which is sufficient for the important conclusions. The results are presented as plots of the velocity vector fields (white arrows) superimposed with images of beads (dark regions) in the microchannels (bright regions) (cf. Figs. 3 and 4). Typically, the vector field plots are averages of 10–15 data sets. The micro-PIV image frames were recorded immediately[1] after turning on the trans-

[1] "Immediately" means approximately a few tenths of a second after turning on the transducer(s). This is well above the time constant, τ, for reaching equilibrium between the radiation force and the viscous drag ($\tau \sim 1$ ms, cf. Section 2.2), and well below the time to reach a static bead distribution in the channel (~10 s).

ducer(s), thus representing the initial and transient motion of beads. In contrast, the bead images were acquired after a few seconds, thus representing the (near-)steady-state distribution of manipulated beads. Finally, in order to investigate and compare the radiation force fields produced by individual transducers, no levitation (in the *y* direction) was performed during the micro-PIV measurements.

4.1.1. Micro-PIV measurements in the Step Chip

In Fig. 3, the results are presented from measurements at the transition region from a 600 μm wide channel (left side) to a 643 μm wide channel (right side) in the Step Chip. In Fig. 3a the 600-μm-wide segment is actuated at 2.62 MHz, in Fig. 3b the 643-μm-wide segment is actuated at 3.51 MHz and in Fig. 3c both segments are actuated simultaneously at 2.62 and 3.51 MHz, respectively. Ideally, each force field should be confined to its corresponding channel segment (cf. Eq. 6). However, in Fig. 3a we see that the resonance "leaks" over to the adjacent channel segment. Although the forces are larger in the left segment, they are still significant in the right segment (i.e., on average a few times smaller to the right than to the left). Thus, a 7%-change in channel width is here not enough for fully confining the resonance to the proposed channel segment. On the other hand, the performance in Fig. 3b is much better in terms of confinement. Here, the forces in the left channel segment are insignificant in comparison to the right segment, and the transition region (defined as the approximately distance from maximum to insignificant forces in the *z* direction) is of the order of $\lambda/4$. Finally, Fig. 3c shows the results when both channel segments are actuated simultaneously. Interestingly, we see here that the "resonance-leakage" into the right segment originating from actuation of the left segment (cf. Fig. 3a) is quenched by the actuation of the right segment. We also note that the vector field in Fig. 3c is not equal to the sum of the vector fields in Fig. 3a and b. For example, the periodic variation of the force along the *z* direction in the right channel segment in Fig. 3c can not be derived from the vector fields in Fig. 3a and b.

4.1.2. Micro-PIV measurements in the Split Chip

In Fig. 4, the results from measurements at one site in the Split Chip are presented. The sub-figures show actuation at 2.94 MHz of the lower right channel segment (Fig. 4a), actuation at 2.10 MHz of the left channel segment (Fig. 4b), and actuation at 2.94 MHz and 2.10 MHz of both segments simultaneously (Fig. 4c). Here, we see almost no "resonance-leakage" (as seen in Fig. 3a). Instead, the fields are well-confined and independent, and with a transition region along the *z*-axis (cf. Section 4.1.1) of the order of $\lambda/2$. In Fig. 4c, we also note the occurrence of areas having velocity fields of rotational character. Such vortices, produced by acoustic streaming, may influence the particle movement in areas with low radiation forces (e.g., in the transition region between two adjacent channel segments).

In order to quantify more accurately the degree of spatial confinement, we have plotted the lateral velocity components (i.e., in the *x* direction in Fig. 4 where the radiation force is strongest) at different *x*-coordinates across the channel width, as a function of the *z*-position (i.e., along the channel direction). In Fig. 5a, the lateral velocities during single-segment actuation are plotted (i.e., the *x* components of the fields shown in both Fig. 4a and b). In Fig. 5b, the lateral velocities during dual-segment actuation are plotted (i.e., the *x* components of the field shown in Fig. 4c). Interestingly, we note that the forces are weaker in the central region (i.e., $\sim$300 μm < *z* < $\sim$600 μm) of the diagram in Fig. 5b, compared to the corresponding region of the diagram in Fig. 5a. Thus, a mutual force-quenching-effect is present in the transition region between the two channel segments during dual-segment actuation. This effect is even more distinct for the Step Chip, where it is directly visible in Fig. 3. Thus, for both chips, the cross-talk between two adjacent channel segments actuated simultaneously seems to have a character of destructive interference and is limited to a region of typical length $\sim\lambda/2$.

4.2. Flow-through operation of the Split Chip

In Fig. 6, we demonstrate flow-through-mode operation at 0.1 μL/s of the Split Chip by the use of up to four simultaneously driven transducers. This chip is designed for two-dimensional alignment and addressable merging of particle tracks. In contrast to the micro-PIV experiments (cf. Sections 4.1 and 4.2), the levitator transducer (cf. the uppermost transducer in Fig. 1a) was operated in all flow-through experiments, resulting in vertical (*y* direction) centering of the particles in the whole channel system. Together with operation of the pre-alignment transducer (cf. Fig. 2), the result is two-dimensional alignment (i.e., simultaneous focusing of particles in both the *x* and y directions), and thus controlled transport of particles in terms of both spatial position and uniform velocity [3]. In the present proof-of-concept chip design, all particles are injected through the one and only inlet for easier fluidic operation. However, depending on the needs from a future application, splitting of the main channel endpoints in several inlets and outlets is straightforward.

Fig. 6a and b shows the effect of actuating the upper left channel segment in flow-through-mode. In Fig. 6a, only the levitator and pre-alignment transducers are activated, and all aligned particles continue in their respective streamline (also in the upper right un-actuated channel segment). In Fig. 6b, the upper left channel segment is actuated, resulting in localized merging of the particle tracks 1 and 2 (cf. denotation in Fig. 2). The images are taken with a long exposure time, making the particles appear as streaks to better visualize their direction of movement. We clearly see that the particle tracks 1 and 2 merge at a distance longer than the $\sim\lambda/2$-distance after which the force in a channel segment was found to reach its full value (cf. Section 4.1). This is the result of the fluid flow giving the particles a considerable velocity component in the *z* direction relative the radiation-force-induced velocity component in the *x* direction. Fig. 6c shows merging of particle tracks 2 and 3 further down the channel by actuation of the lower left channel segment (cf. Fig. 2). This experiment was performed without any preceding merging of particle tracks 1 and 2. Finally, all particle tracks (two or three, depending on whether any of the above merging steps is performed) can be merged by actuation of the final channel segment (cf. Fig. 2).

5. Discussion and conclusions

In this section, we will consider channel design strategies for implementing several localized manipulation functions in series along a microchannel by the use of ultrasonic standing wave (USW) technology in a microfluidic chip. Ideally, each manipulation function should be represented by a localized and spatially confined force field that can be independently addressed by a frequency-specific external transducer. Furthermore, the overlap or cross-talk between the force fields of two adjacent manipulation functions should be minimized. Below we outline design criteria for advanced particle handling and processing chips based on our experimental observations.

When actuating a single-channel segment in both the Step Chip and the Split Chip, we may conclude that each primary radiation force field F_{PR} is localized to its corresponding segment (cf. Figs. 3 and 4). At the beginning and the end of each segment, there is an intermediate area of force field gradient (from insignificant to full value of the forces) with typical length $\lambda/4 - \lambda/2$ (where λ is the acoustic wavelength in the fluid). However, one exception to

this degree of confinement is seen in Fig. 3a, where the force field gradient in the z direction outside the actuated channel segment is very small. The result is a resonance that "leaks" out into the rest of the fluid channel. We believe that one reason for this poor confinement could be bad matching between the transducer resonance and the channel resonance. As a comparison, for a conventionally designed one-dimensional layered resonator (where the transducer is an active part of the resonator), the forces are typically halved if the driving frequency is changed with only 0.5% from a resonance peak [26]. In Fig. 3, the change in channel width corresponds to a change in resonance frequency of 7%. Thus, given a similar performance in our chip as in Ref. [26], we would not expect any forces of significance outside the actuated channel segment. On the other hand, if the channel segments are considered separately it is also possible that the wider channel segment in Fig. 3a is wide enough to be close to another resonance peak than the peak in the thinner segment. For example, when tuning the actuation frequency for a certain channel segment there are typically several resonance frequencies separated with similar (relative) steps as the relative change in channel width in Fig. 3. Thus, we believe that similar resonances would be found if we could "tune" the channel segment width at a fixed frequency (cf. e.g., Ref. [27]). One simple design strategy to avoid resonance leakage is to employ much larger steps in channel width, as demonstrated in the Split Chip.

When two adjacent channel segments are actuated simultaneously by the use of two transducers operating at different frequencies, we conclude that no cross-talk of significance (for the performance of each manipulation function) occurs in neither of the two chips. Typically, there is a near-force-free transition region between the manipulation functions of length $\sim\lambda/4$ in the Step Chip (cf. Fig. 3c), and $\sim\lambda/2$ in the Split Chip (cf. Figs. 4c and 5). The reason for the longer transition region in the Split Chip is due to the gradually (and not stepwise) increasing channel width in that chip. However, it is important to note that the sum of the force fields during single-segment actuation is not equal the force field during dual-segment actuation. Minor field coupling effects are visible in Figs. 3 and 4, e.g., periodic force variations in the z direction (along the channel), acoustic-streaming-induced vortices in low-force regions, and mutual quenching of "leaky" resonances in the intermediate area between the segments. Neither of these effects causes any reduction in performance of significance of a particle handling/processing chip based on several spatially separated manipulation functions (as demonstrated in e.g., Fig. 6).

Finally, it should be noted that the radiation forces are not constant throughout the segment (i.e., along the z-axis) to which it is confined. There will be periodically recurring areas where the focusing component of the force is very weak, or indeed is almost equal to zero. Actually, this is a general effect that is visible during both single- and multi-segment actuation. The reason is that we do not solely have a simple standing wave in the channel, but rather a three-dimensional resonance which exists in the whole chip structure, including all supporting layers to the fluid channel (such as the silicon layer, the glass layers, the external transducers, and even the microscope chip holder). While it is possible to design the system so that the force field is considerably confined, the rest of the chip will still influence the actual shape of the confined field. Finite-element simulations on our chips (data not shown) using the method described in Ref. [18] predict the existence of such areas, which are confirmed in our experiments (cf. e.g., Fig. 3c) but also in other reports (see e.g., Refs. 18,22,28). The influence of the entire chip (in terms of material choices and geometry) on the resonance shape is the underlying reason for this phenomenon. For example, a simple and straight half-wavelength channel does not focus particles into a straight line, but rather into slightly curved lines and at some places not at all under static (no-flow) conditions. However, this effect is often not visible in flow-through applications for several reasons. Firstly, the laminar flow profile will cause a particle to simply follow its streamline through areas where the forces are low. Secondly, any effect on the bead movement due to the force asymmetry around curved nodes is typically cancelled out in flow-through-mode. In our suggested flow-through application (cf. Section 4.2), these effects will be of little or no importance for the performance of the chip. However, for a chip designed for no or very low flow, or designed for retention of particles in a flow, the effects must be considered as a part of the design process.

Acknowledgements

The authors would like to thank Peder Skafte-Pedersen at MIC/DTU for his simulations of resonances in the chip. This paper was generated in the context of the *CellPROM* project, funded under the 6th Framework Program of the European Community (Contract No.: NMP4-CT-2004-500039). The work was also supported by the Swedish Research Council for Engineering Sciences.

References

[1] M. Wiklund, H.M. Hertz, Ultrasonic enhancement of bead-based bioaffinity assays, Lab Chip 6 (2006) 1279–1292.
[2] T. Laurell, F. Petersson, A. Nilsson, Chip integrated strategies for acoustic separation and manipulation of cells and particles, Chem. Soc. Rev. 36 (2007) 492–506.
[3] O. Manneberg et al., Elementary manipulation functions for gentle and long-term handling of cells in microchannels by ultrasonic standing waves, Proc. of Nanotech-Montreux 2006, Montreux, Switzerland, 2006.
[4] T. Müller, A. Pfennig, P. Klein, G. Gradl, M. Jäger, T. Schnelle, The potential of dielectrophoresis for single-cell experiments, IEEE Eng. Med. Biol. 22 (2003) 51–61.
[5] J. Enger, M. Goksör, K. Ramser, P. Hagberg, D. Hanstorp, Optical tweezers applied to a microfluidic system, Lab Chip 4 (2004) 196–200.
[6] M. Wiklund, C. Günther, R. Lemor, M. Jäger, G. Fuhr, H.M. Hertz, Ultrasonic standing wave manipulation technology integrated into a dielectrophoretic chip, Lab Chip 6 (2006) 1537–1544.
[7] J. Hultström, O. Manneberg, K. Dopf, H.M. Hertz, H. Brismar, M. Wiklund, Proliferation and viability of adherent cells manipulated by standing-wave ultrasound in a microfluidic chip, Ultrasound Med. Biol. 33 (2007) 145–151.
[8] J. Svennebring, O. Manneberg, M. Wiklund, Temperature regulation during ultrasonic manipulation for long-term cell handling in a microfluidic chip, J. Micromech. Microeng. 17 (2007) 2469–2474.
[9] J.J. Hawkes, W.T. Coakley, Force field particle filter, combining ultrasound standing waves and laminar flow, Sens. Actuator B-Chem. 75 (2001) 213–222.
[10] N.R. Harris, M. Hill, S. Beeby, Y. Shen, N.M. White, J.J. Hawkes, W.T. Coakley, A silicon microfluidic ultrasonic separator, Sens. Actuator B-Chem. 95 (2003) 425–434.
[11] K. Yasuda, Non-destructive non-contact handling method for biomaterials in micro-chamber by ultrasound, Sens. Actuator B-Chem. 64 (2000) 128–135.
[12] S. Kapishnikov, V. Kantsler, V. Steinberg, Continuous particle size separation and size sorting using ultrasound in a microchannel, J. Stat. Mech. P01012 (2006) 1–15.
[13] A. Haake, J. Dual, Positioning of small particles by an ultrasound field excited by surface waves, Ultrasonics 42 (2004) 75–80.
[14] T. Lilliehorn, U. Simu, M. Nilsson, M. Almqvist, T. Stepinski, T. Laurell, J. Nilsson, S. Johansson, Trapping of microparticles in the near field of an ultrasonic transducer, Ultrasonics 43 (2005) 293–303.
[15] T. Lilliehorn, M. Nilsson, U. Simu, S. Johansson, M. Almqvist, J. Nilsson, T. Laurell, Dynamic arraying of microbeads for bioassays in microfluidic channels, Sens. Actuator B-Chem. 106 (2005) 851–858.
[16] M. Evander, L. Johansson, T. Lilliehorn, J. Piskur, M. Lindvall, S. Johansson, M. Almqvist, T. Laurell, J. Nilsson, Noninvasive acoustic cell trapping in a microfluidic perfusion system for online bioassays, Anal. Chem. 79 (2007) 2984–2991.
[17] J.G. Santiago, S.T. Wereley, C.D. Meinhart, D.J. Beebe, R.J. Adrian, A particle image velocimetry system for microfluidics, Exp. Fluids 25 (1998) 316–319.
[18] S.M. Hagsäter, T. Glasdam Jensen, H. Bruus, J.P. Kutter, Acoustic resonances in microfluidic chips: Full-image micro-PIV experiments and numerical simulations, Lab Chip 7 (2007) 1336–1344.
[19] M. Gröschl, Ultrasonic separation of suspended particles – Part I: fundamentals, Acta Acustica 84 (1998) 432–447.
[20] L.P. Gor'kov, On the forces acting on a small particle in an acoustic field in an ideal fluid, Sov. Phys. Doklady 6 (1962) 773–775.
[21] M. Wiklund, Ultrasonic enrichment of microparticles in bioaffinity assays, PhD Thesis, Royal Institute of Technology (2004) ISBN 91-7283-723-3.

[22] S. Oberti, A. Neild, J. Dual, Manipulation of micrometer sized particles within a micromachined fluidic device to form two-dimensional patterns using ultrasound, J. Acoust. Soc. Am. 121 (2007) 778–785.
[23] H. Bruus, Theoretical Microfluidics, Oxford University Press, Oxford, 2007.
[24] L.K. Zarembo, Acoustic streaming, in: L.D. Rozenberg (Ed.), High-Intensity Ultrasonic Fields, Plenum Press, New York, 1971, pp. 138–199. vol. 85, part 3.
[25] S.M. Hagsäter, C.H. Westergaard, H. Bruus, J.P. Kutter, Investigations on LED illumination for micro-PIV including a novel front-lit configuration, Exp. Fluids 44 (2008) 211–219.
[26] M. Hill, The selection of layer thicknesses to control acoustic radiation force profiles in layered resonators, J. Acoust. Soc. Am. 114 (2003) 2654–2661.
[27] M. Wiklund, J. Toivonen, M. Tirri, P. Hänninen, H.M. Hertz, Ultrasonic enrichment of microspheres for ultrasensitive biomedical analysis in confocal laser-scanning fluorescence detection, J. Appl. Phys. 96 (2004) 1242–1248.
[28] S.M. Hagsäter, A. Lenshof, P. Skafte-Pedersen, J.P. Kutter, T. Laurell, H. Bruus, Acoustic resonances in straight micro channels: beyond the 1D-approximation, Lab Chip (2008). doi: 10.1039/b801028e.